Supporting Information for "Engineering the Mechanical Properties of Monolayer Graphene Oxide at the Atomic Level"

Rafael A. Soler-Crespo[1,†], Wei Gao[1,2,†], Penghao Xiao[3], Xiaoding Wei[1,2], Jeffrey T. Paci[4,5], Graeme Henkelman[3], Horacio D. Espinosa[1,2,*]

[†] These authors contributed equally to this work

* espinosa@northwestern.edu

1. Theoretical and Applied Mechanics Program, Northwestern University, 2145 Sheridan Road, Evanston, IL 60208, USA
2. Department of Mechanical Engineering, Northwestern University, 2145 Sheridan Road, Evanston, IL 60208, USA
3. Department of Chemistry and the Institute for Computational Engineering and Sciences, The University of Texas at Austin, Austin, Texas 78712-0165, USA
4. Department of Chemistry, Northwestern University, 2145 Sheridan Road, Evanston, IL 60208, USA
5. Department of Chemistry, University of Victoria, British Columbia, V8W 3V6, Canada

1. Computational Methods

2 x 2 nm^2 graphene oxide (GO) models with different compositions, *i.e.,* varying functional group ratios while maintaining a constant 70% degree of oxidation, were prepared utilizing the proposed Monte Carlo-based Rosenbluth sampling algorithm as presented elsewhere[1, 2], which accounts for the stochastic oxidation process involved during sample synthesis[1, 3]. Then, the generated models were subjected to a simulated, molecular mechanics (MM) based, displacement controlled tensile experiment by applying uniaxial strain tension along the armchair direction (*i.e.,* tensile strain was applied in the armchair direction, with the zigzag direction atoms held fixed). Simulations were performed in CP2K (https://www.cp2k.org/) utilizing the *mio-0-1* Slater-Koster parameter set and charge self-consistency[4], as implemented. Charges were treated utilizing a smooth-particle mesh Ewald (SPME) summation, with one grid point per Å. The Ewald convergence parameter was set to 0.35, and a cutoff radius of 10 Å for the real-space forces was used. Displacements of the unit-cell boundaries were prescribed utilizing 0.5% strain increments between strain steps. Geometry optimizations were performed between steps. Stress measures were obtained by calculating virial stresses according to the virial theorem, as implemented in CP2K.

Further supporting simulations (with specific functional group ratios but varying degrees of oxidation) performed for validation and completeness are subjected to three different displacement controlled conditions: uniaxial strain tension along the i) armchair (*i.e.,* tensile strain was applied in the armchair direction, with the zigzag direction atoms held fixed) and ii) zigzag directions, and iii) equibiaxial strain tension. Simulations were performed by following the same method outlined previously.

In addition to DFTB simulations, we also applied density functional theory (DFT) calculations to verify the DFTB method (see Supplemental Section 2). All the DFT calculations in this study were performed using the plane-wave-based Vienna Ab-initio Simulation Package (VASP)[5, 6]. Projector augmented waves (PAW)[7, 8] were used to represent ionic cores, and the electronic kinetic energy cutoff for the plane-wave basis describing the valence electrons was set to 520 eV. A 5 × 5 × 1 k-point mesh was used for calculations.

2. Validation of DFTB theory based on DFT results

Due to the large number of systems of interest in this study, simulations that rely on a high level of theory such as DFT would become prohibitively expensive. Instead, and to circumvent this challenge, we opted to utilize a DFTB approach to both quickly and accurately screen the material space accessible to GO (wherein multiple chemical compositions can exist for a given degree of oxidation), and extract material properties of interest. To validate the DFTB approach, we compared the in-plane stress-strain behavior of a specific GO sheet with a single epoxide functional group. Our main focus during this exercise was to examine the accuracy of DFTB as compared to DFT in predicting mechanical properties (*e.g.,* Young's modulus and strength) and deformation mechanisms (*e.g.,* epoxide-to-ether transformations) of the same model system. It is important to note that DFTB has been previously shown to compare favorably with experiments[2, 4, 9, 10].

As shown in Figure S1, DFT and DFTB are comparable and capture critical deformation mechanisms present in the system. For instance, Figure S1a shows a load drop for both DFT and DFTB, corresponding to an epoxide-to-ether transformation of the functional group in the material, albeit at different stress levels. The strength, failure strain and failure mechanisms

along the armchair (Figure S1a) and zigzag (Figure S1b) directions are similar for the case considered.

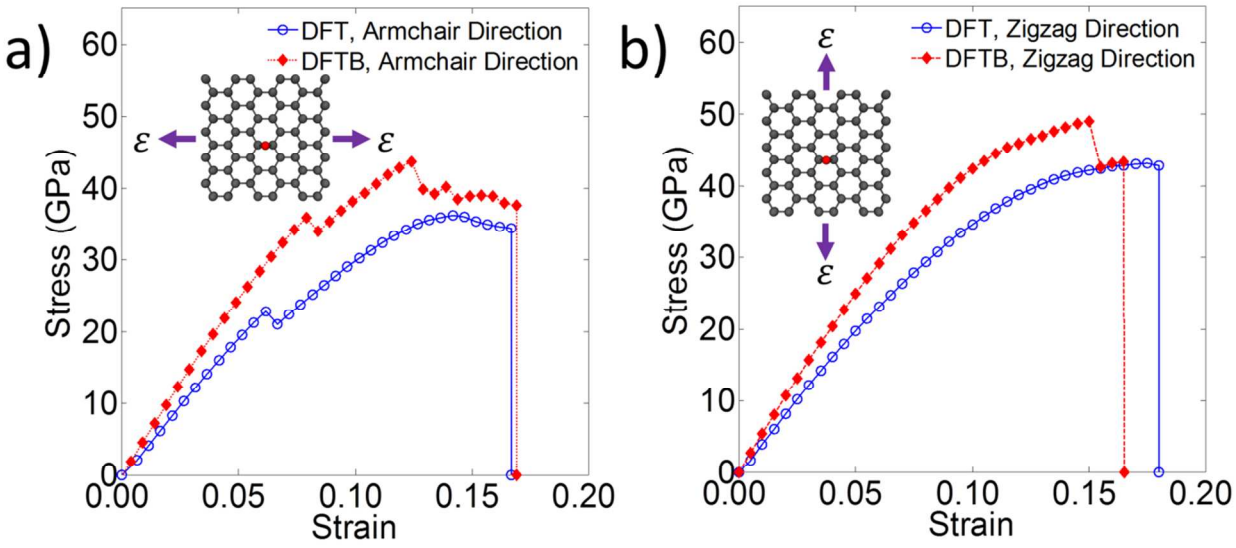

Figure S1. (a-b) Stress-strain response comparison between density functional theory (DFT) and the density functional-based tight binding (DFTB) method for a 1 x 1 nm^2 graphene oxide system along the (a) armchair and (b) zigzag directions.

As noted in the article, for all the properties of interest in our study (*i.e.,* Young's modulus, strength, toughness), DFTB shows a consistent stiffening of the system when compared to DFT. This is not surprising based on previous reports on carbon nanomaterials that rely on DFTB calculations[9] and the assumptions made to enhance the efficiency of the method[10]. Nonetheless, and given the reasonable agreement between DFT and DFTB in terms of mechanical properties and deformation mechanisms observed in the material, and the good agreement with experimental findings, we opted to utilize DFTB for our study to benefit from the computational efficiency afforded by the method for the large number of simulations performed in this study.

3. Analysis of mechanical properties

After obtaining the stress-strain response of various GO sheets utilizing the DFTB molecular mechanics simulations employed in this study, we extracted various mechanical properties of

interest from the system. To extract linear elastic properties (*e.g.,* Young's modulus), we obtained estimates for the material elastic constants. Based on previous theoretical and experimental studies, we assume that the material is isotropic linear elastic such that the following relationships hold:

$$E = \frac{C_{11}^{\ 2} - C_{12}^{\ 2}}{C_{11}} \tag{1}$$

where E is the elastic modulus of the system, and C_{11} and C_{12} are elastic constants.

For each of the uniaxial strain tension results obtained in this study, a set of elastic constants, C_{11} and C_{12} was determined through least-squares fitting of the initial part of the stress-strain curves (*i.e.,* low-strain regime). The two obtained constant determine an elastic modulus along the strained direction independently. Non-linearities in the stress-strain curves at small strains arise mainly from increasing waviness in the system as the degree of oxidation increases, intrinsic in the sheet due to their highly oxidized nature. To alleviate this artifact, stress-strain curves were linearized according to regions where the tangential slope became stable and shifted horizontally such that the linear extrapolation of the curves passed through the origin.

The toughness (Γ) of GO was computed by integrating the stress-strain curve according to the definition:

$$\Gamma = \int_0^{\varepsilon_f} \sigma d\varepsilon \tag{2}$$

Integration of the stress-strain curves was performed using the trapezoidal rule on the as-obtained data set.

4. Mechanical properties of GO as a function of composition

To understand the mechanics of graphene oxide as a function of its composition, various models with a 70% degree of oxidation and varying epoxide-to-hydroxyl functional group ratio were generated in this study, as previously discussed. Representative stress-strain curves for the generated models are shown in Figure S2 (obtained by performing uniaxial tensile strain along the armchair direction), capturing the general behavior of the material.

Consistent with the main findings of this report, as epoxide content was increased (*i.e.,* δ increased), the ductility (represented by strain to failure) and toughness of the system increased while maintaining material strength and Young's modulus approximately constant. It is important to note that while the strain burst associated with epoxide-to-ether transformations is not present for all stress-strain curves (see Figure S2, in particular, the cases for δ = 0.50 and 0.75), the transformation does occur before the first load drop as observed by tracking the atomic positions of the system. In general, as δ increases, GO tends to become more ductile and display hardening behavior, consistent with previous reports[2, 11] and the observations made in this study.

The models utilized for generating the stress-strain curves in Figure 1 of the main text, *i.e.,* hydroxyl- and epoxide-rich GO sheets, were also subjected to equibiaxial strain tension and uniaxial strain tension along the zigzag direction, to show the generality of the observations made in this report. Figure S3a and Figure S3b show the stress-strain response of hydroxyl- and epoxide-rich GO to uniaxial strain tension along the zigzag direction and equibiaxial strain tension, respectively. In general, the behavior of hydroxyl-rich GO remains brittle independent of the loading condition.

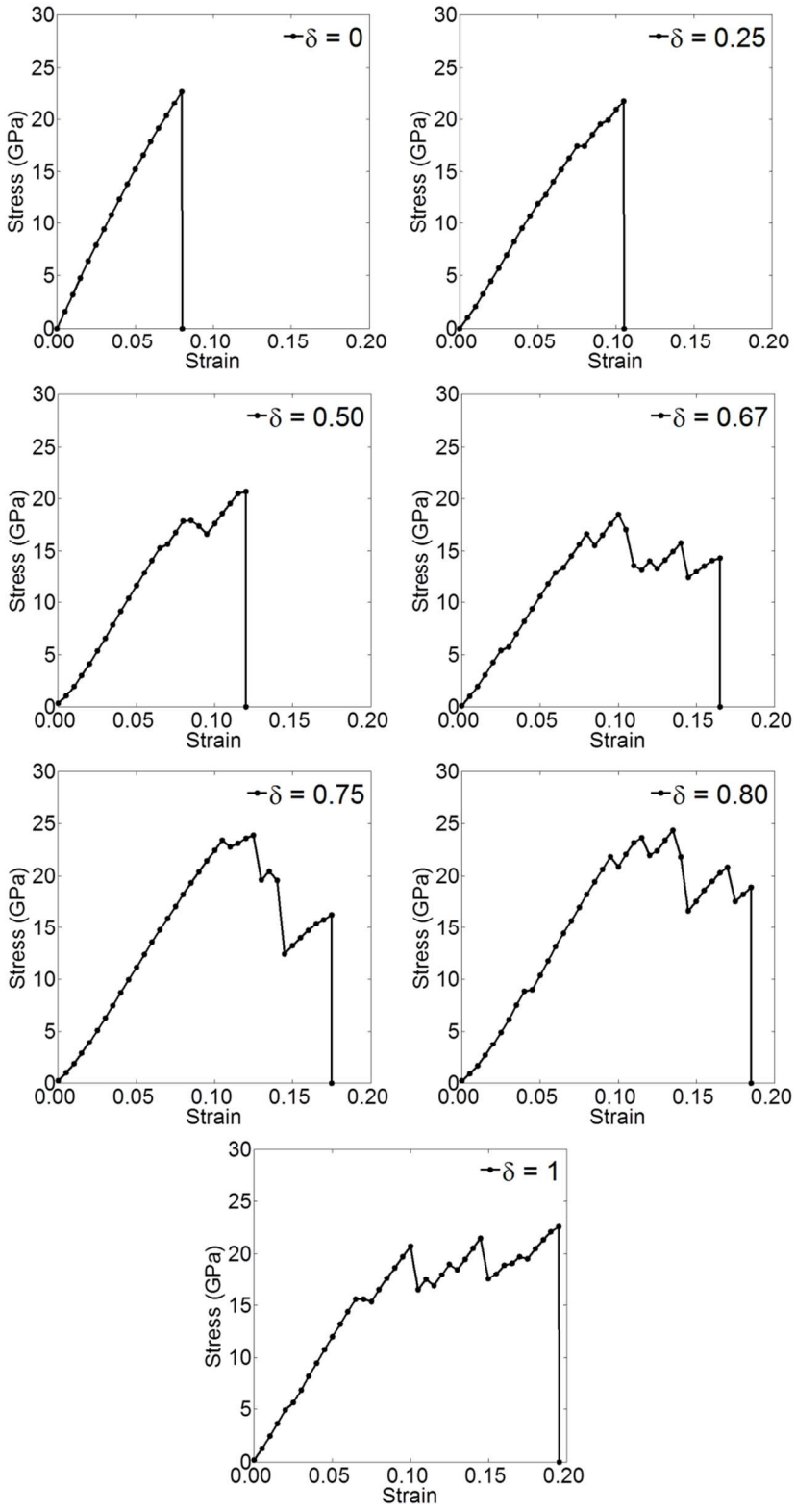

Figure S2. Representative stress-strain curves for graphene oxide sheets with a 70% degree of oxidation and varying epoxide-to-hydroxyl functional group ratio, δ.

Conversely, epoxide-rich GO is shown to be ductile independently of the loading conditions applied. It is important to note that the strength of GO appears to be substantially lower during equibiaxial strain tension due to the complicated stress state imposed in the material, which is typical for most materials.

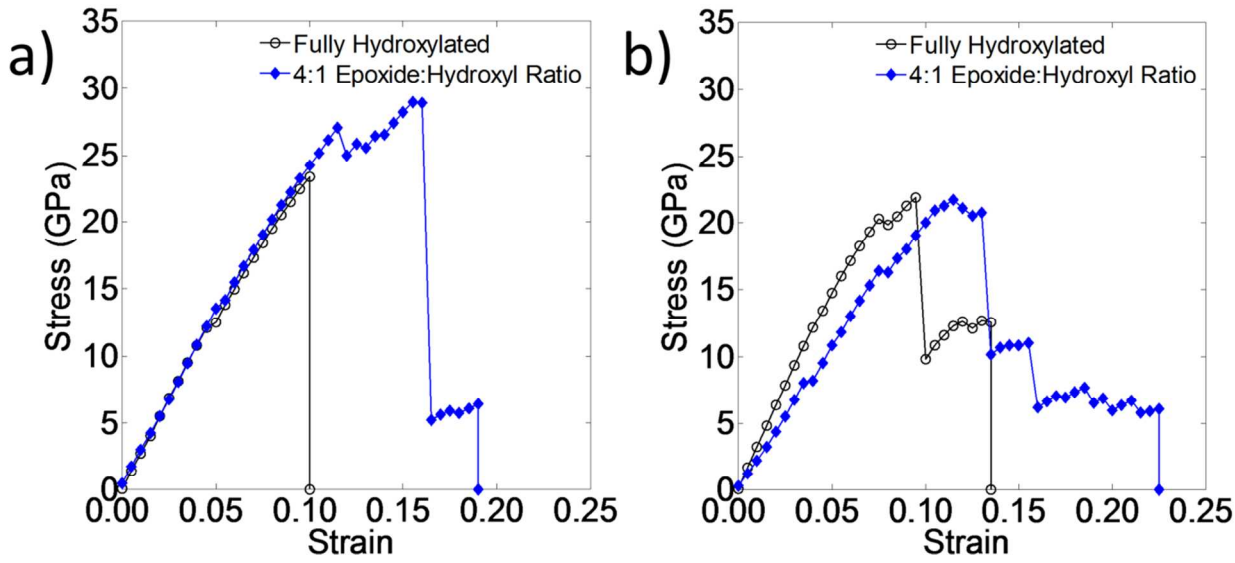

Figure S3. Representative stress-strain curves for hydroxyl- and epoxide-rich graphene oxide, tested in (a) uniaxial strain tension along the zigzag direction and (b) equibiaxial strain tension.

The spatial distribution of functional groups can also be thought to affect the material properties of the system. To verify this effect, and as discussed in the manuscript, five GO sheets were tested for this particular study at each degree of oxidation, for each chemical composition. Table S1 shows a representative set of properties for a system with a 70% degree of oxidation and a 1:1 epoxide:hydroxyl functional group ratio (*i.e.* δ is 0.5). Since the magnitude of the standard deviation is small when compared to the magnitude of the properties themselves, it is possible to consider the spatial distribution of functional groups in GO as a second-order effect. This is further reflected by the fact that similar effects are observed for calculations where the degree of oxidation is the same, but chemical composition is significantly different.

Table S1. Mechanical properties for GO sheets with a 70% degree of oxidation and a 1:1 epoxide:hydroxyl functional group ratio, with different functional group spatial distributions.

System	Elastic Modulus (GPa)	Strength (GPa)	Toughness (GJ/m^3)
1	253.4	20.7	1.46
2	285.1	26.5	1.60
3	287.3	22.5	1.74
4	264.8	23.2	1.60
5	271.9	24.8	1.58

5. Study on the bond strength of functional groups in GO

As part of our analysis, due to discovering that the strength of GO at a given degree of oxidation is seemingly independent of the composition of the material, we investigated the influence of different functional groups in the strength of GO.

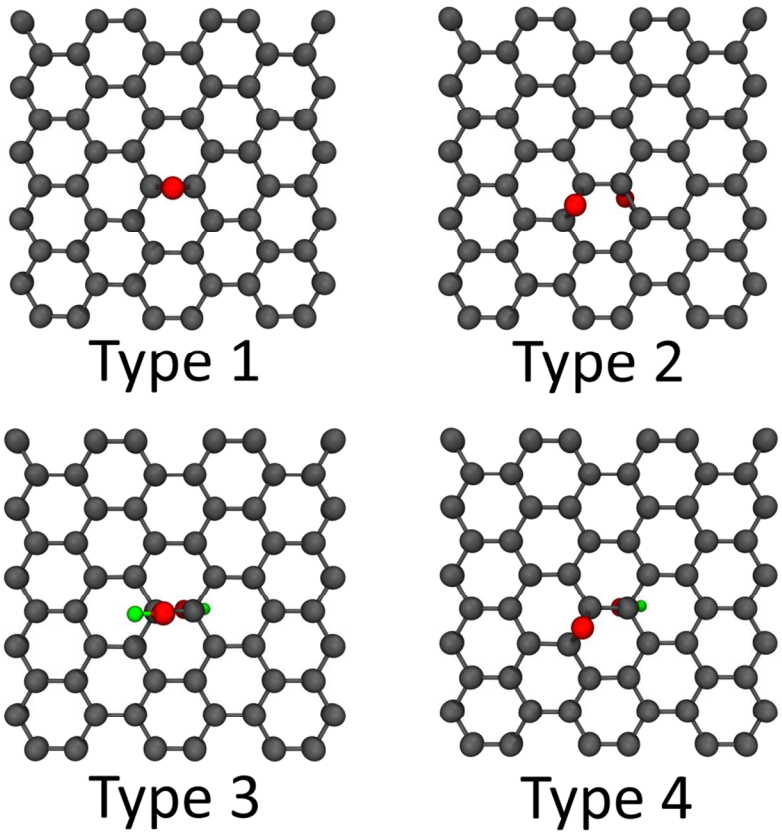

Figure S4. Graphene oxide models with one bond type per system. Models were used to study the effect of bond type in the strength of a graphene backbone, as shown in Figure 5 of the manuscript.

An analysis of the microstructure of GO revealed the presence of four combination of functional groups, which we define as “bond types”, which may determine material strength. To isolate the effect of these functional groups in material strength, we constructed representative GO structures functionalized with only one of these combinations of functional groups – i.e., bond types – and applied uniaxial tensile strain along the armchair direction to simulate a mechanical experiment. The data obtained from this study is shown in Figure 5 of the manuscript, and the atomistic structures used to perform this study are shown in Figure S4.

References

1. Paci, J. T.; Belytschko, T.; Schatz, G. C. Computational studies of the structure, behavior upon heating, and mechanical properties of graphite oxide. *J. Phys. Chem. C* **2007,** *111*, 18099-18111.
2. Wei, X.; Mao, L.; Soler-Crespo, R. A.; Paci, J. T.; Huang, J.; Nguyen, S. T.; Espinosa, H. D. Plasticity and ductility in graphene oxide through a mechanochemically induced damage tolerance mechanism. *Nat. Commun.* **2015,** *6,* 8029.
3. Erickson, K.; Erni, R.; Lee, Z.; Alem, N.; Gannett, W.; Zettl, A. Determination of the local chemical structure of graphene oxide and reduced graphene oxide. *Adv. Mater.* **2010,** *22*, 4467-4472.
4. Elstner, M.; Porezag, D.; Jungnickel, G.; Elsner, J.; Haugk, M.; Frauenheim, T.; Suhai, S.; Seifert, G. Self-consistent-charge density-functional tight-binding method for simulations of complex materials properties. *Phys. Rev. B* **1998,** *58*, 7260-7268.
5. Kresse, G.; Furthmuller, J. Efficient iterative schemes for ab initio total-energy calculations using a plane-wave basis set. *Phys. Rev. B* **1996,** *54*, 11169-11186.
6. Kresse, G.; Hafner, J. Ab initio molecular dynamics for liquid metals. *Phys. Rev. B* **1993,** *47*, 558-561.
7. Blochl, P. E. Projector augmented-wave method. *Phys. Rev. B* **1994,** *50*, 17953-17979.
8. Kresse, G.; Joubert, D. From ultrasoft pseudopotentials to the projector augmented-wave method. *Phys. Rev. B* **1999,** *59*, 1758-1775.
9. Zhao, H.; Min, K.; Aluru, N. Size and chirality dependent elastic properties of graphene nanoribbons under uniaxial tension. *Nano Lett.* **2009,** *9*, 3012-3015.
10. Frauenheim, T.; Seifert, G.; Elstner, M.; Niehaus, T.; Köhler, C.; Amkreutz, M.; Sternberg, M.; Hajnal, Z.; Di Carlo, A.; Suhai, S. Atomistic simulations of complex materials: ground-state and excited-state properties. *J. Phys. Condens. Matter* **2002,** *14*, 3015-3047.
11. Cao, C.; Daly, M.; Singh, C. V.; Sun, Y.; Filleter, T. High strength measurement of monolayer graphene oxide. *Carbon* **2015,** *81*, 497-504.